Biomicrofluidics ARTICLE scitation.org/journal/bmf

A microfluidic flow analyzer with integrated lensed optical fibers

Cite as: Biomicrofluidics 14, 054104 (2020); doi: 10.1063/5.0013250
Submitted: 12 May 2020 · Accepted: 14 September 2020 ·
Published Online: 1 October 2020

A. Mohan,[1,a)] P. Gupta,[2] A. P. Nair,[2] A. Prabhakar,[1] and T. Saiyed[2]

AFFILIATIONS

[1]Department of Electrical Engineering, Indian Institute of Technology Madras (IITM), Chennai 600036, India
[2]Discovery Innovation Accelerator, Centre for Cellular and Molecular Platforms (C-CAMP), Bengaluru 560065, India

[a)]**Author to whom correspondence should be addressed:** ee14d300@ee.iitm.ac.in and anilpr@ee.iitm.ac.in

ABSTRACT

Rapid optical interrogation of flowing cells or particles is a powerful tool in the field of biomedical diagnostics. Determination of size and composition of fast-flowing cells, with diameters in the range of 2–15 μm, often require complex open-space optics and expensive high-speed cameras. In this work, a method to overcome these challenges by using a hydrodynamic flow-based microfluidic platform coupled with on-chip integrated fiber optics is reported. The lab-scale portable device developed uses a combination of on-chip lensed and non-lensed optical fibers for precision illumination. The narrow light beam produced by the lensed fiber ($f = 150\,\mu$m) enables precise optical analysis with high sensitivity. A planar arrangement of optical fibers at various angles facilitates multi-parametric analysis from a single point of interrogation. As proof of concept, the laboratory-scale portable bench-top prototype is used to measure fluorescence signals from CD4 immunostained cells and human blood samples. The performance of microfluidic flow analyzer is also compared to the conventional Guava® easyCyte 8HT flow cytometer.

I. INTRODUCTION

Rapid diagnostics and treatment facilities are always in demand, and the underlying technology platforms must be constantly upgraded to stay abreast of the changing needs. A quick analysis and a high sensitivity are both important requirements for point-of-care (POC) diagnostic devices. Flow cytometry has always been a trusted workhorse for clinical diagnostics but has also been equally available in biomedical research fields such as immunology, cancer biology, etc. However, current state-of-the art flow analyzers are costly, require frequent maintenance, and need trained technicians to operate the instrument. This makes it difficult to avail them in every primary health care unit, particularly in rural areas and other resource-limited settings. There have been several attempts to miniaturize the flow analyzer for use as a POC diagnostic device.[1–4] Many of these development efforts have relied on optofluidic lab-on-chip devices, where researchers combine the principles of optics, flow cytometry, microfluidics chip fabrication, and microelectronics to allow rapid sample analysis and quantification.[5–13]

Cytometric measurements are usually performed on a single file flow of cells/particles in flow cytometers.[14] Typically, a stream of cells is steered down a flow channel, where each cell undergoes an optical interrogation by a laser at a desired wavelength. Signals coming out of this interrogation are recorded by optical detectors kept at different angles yielding important physical and chemical information from each cell/particle. The optical interrogation requires well aligned light focusing and collection optics, which can capture weak signals with precision. Current systems typically employ free-space optics consisting of multiple lasers, lenses, prisms, filters, high gain detectors, etc., which brings in bulkiness and complexity and adds cost.

While some of the existing miniaturized systems offer good signal acquisition in biological samples, they still require a complex multi-step fabrication process and even use expensive equipment like high-end fluorescence microscopes.[15–19] Optical fibers have been previously used to avoid free-space coupling with and without the use of on-chip embedded lenses.[5–9,20,21] A few on-chip lens systems have been devised to circumvent the problem and focus the beam of light from the optical fiber tip but they often require higher optical power to overcome the losses at the interfaces. In order to bring diagnostic solutions for easier use by the people, the current microfluidic platforms must become amenable to large scale manufacturing and subsequent use as point of care (POC) diagnostic devices.[22]

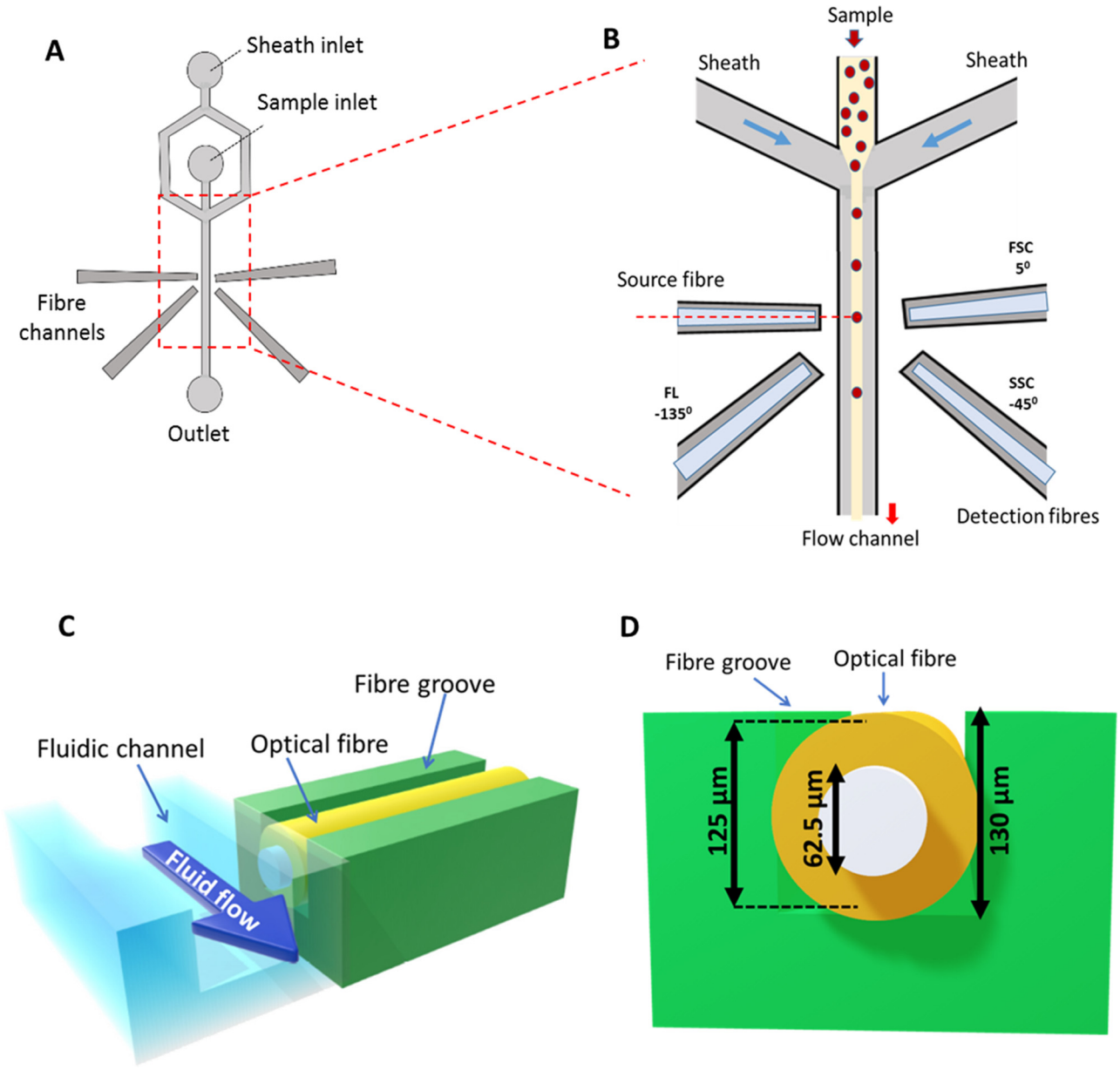

FIG. 1. Microfluidic flow analyzer device design. (a) Schematic diagram of the microfluidic chip design. (b) Inset cross section of the device at interrogation point. The sheath flow from two sides hydro-dynamically focuses the flow of the sample containing cells into a uniform central stream. Optical fibers inserted in the fiber channels at the cross section are used for light illumination and collection of optical signals from the cells passing the path of light. Different optical properties are inferred from signals collected at different angles with reference to the source fiber. (c) Cross section view of central flow channel and fiber groove arrangement, both having a depth of 130 μm. (d) Cross-sectional view of the fiber alignment within the groove.

Our method here simplifies the system with a simple 2D microfluidic platform and an effective combination of lensed single mode fibers (SMFs) with non-lensed multimode fibers (MMFs) for efficient optical illumination and detection of signals, respectively. Use of a lensed SMF provides confinement of the laser beam to a small spot, eliminating the need of focusing lenses or beam shaping prisms. Similarly, the use of a multimode non-lensed fiber for detection end improves the collection of light into the detector. This combination of single mode and multimode optical fibers when used in the right selection of angles makes the system robust.

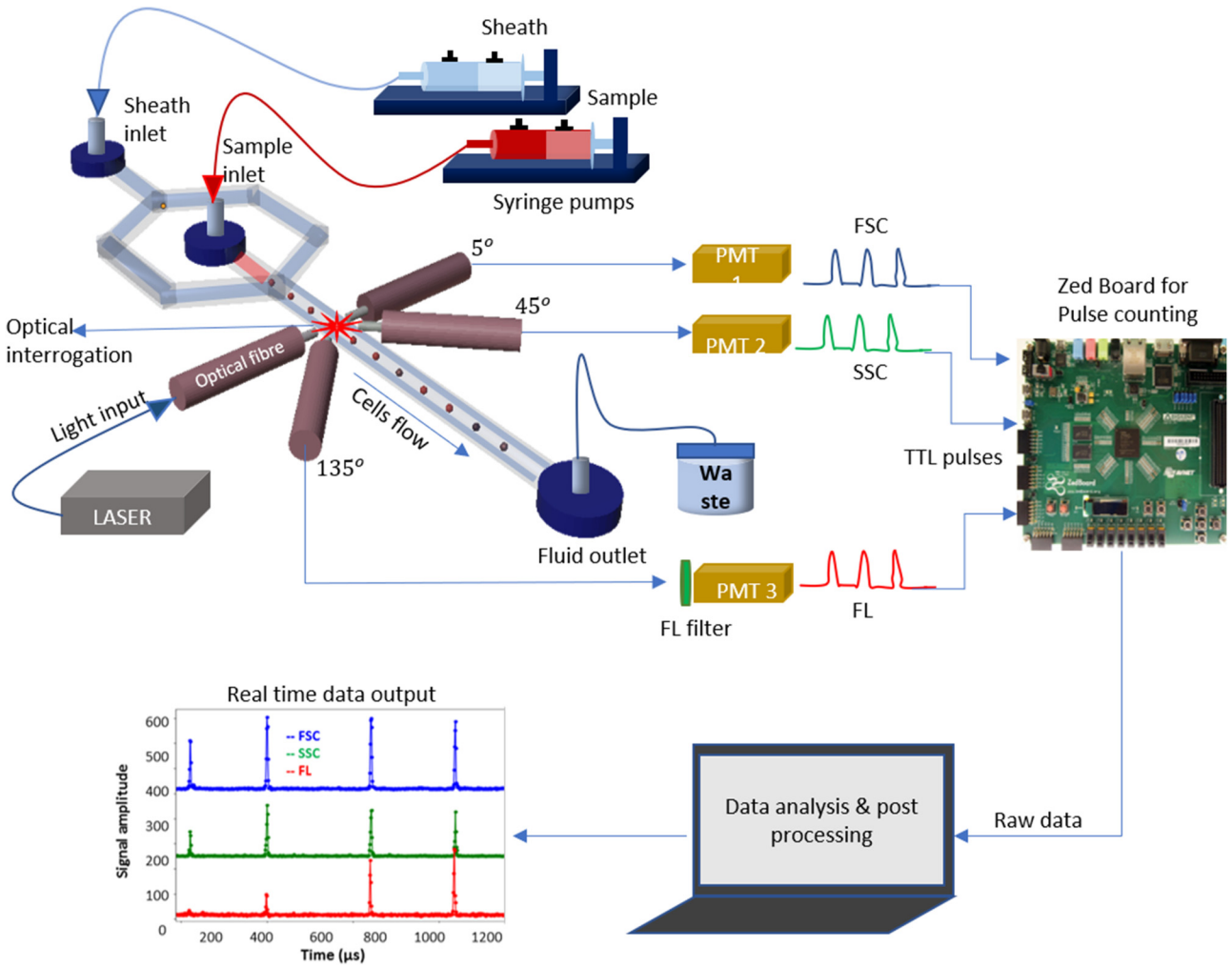

FIG. 2. The microfluidic flow analyzer setup. Two syringe pumps are used to control the flow rates of sample and sheath fluids. Optical fiber coupled to a laser is used to illuminate cells in the flow channel. Light scattered off the cell and emitted fluorescence signals are collected using optical fibers coupled to detectors followed by the pulse processing Zed Board. Collected data are analyzed and processed to get FSC, SSC, and FL values of cells.

In our design, we account for the refraction at the different angles of collection and the numerical aperture (NA) of the fiber before deciding upon the optimal combination.

Very much like a conventional flow cytometer, our microfluidic flow analyzer (MFA) allows simultaneous collection of small angle forward scattered light (FSC) indicative of cell size, larger angle side scattered light (SSC) indicative of internal cellular composition and fluorescence (FL).[14,23,24] These scattered light and fluorescent signals are used to characterize different cell types in a heterogeneous cell population. Fluorescence intensity measurement from cells labeled with fluorescent dyes or fluorescent-tagged antibodies specific to a cellular protein is further used for analyzing the expression of cellular bio-markers. Estimation of the presence of or changes in bio-marker expression, in turn, provides a critical parameter for diagnosing disease conditions.[25–28]

In the MFA, a chosen laser detects the presence of specific bio-markers and associated software gives the measure of these bio-markers in patient samples. The same technology can also be adapted to other diagnostic assays, such as blood count assays, cell culture assays, detection of water contamination, oncological tests, stem cell assays, etc. The final instrument prototype that uses low sample volume is highly portable, cheaper, and easier to maintain and upgrade. With accurate flow velocities and timing characterization, we can also create multiple interrogation points with multiple lasers coupled into additional fiber channels on the microfluidic chip, thus expanding the range of excitation and detection.

The present work focuses on demonstrating the functionality of the MFA for cytometric measurement of different biological samples. We are able to separate polystyrene beads of differing sizes and have also demonstrated the capability of measuring

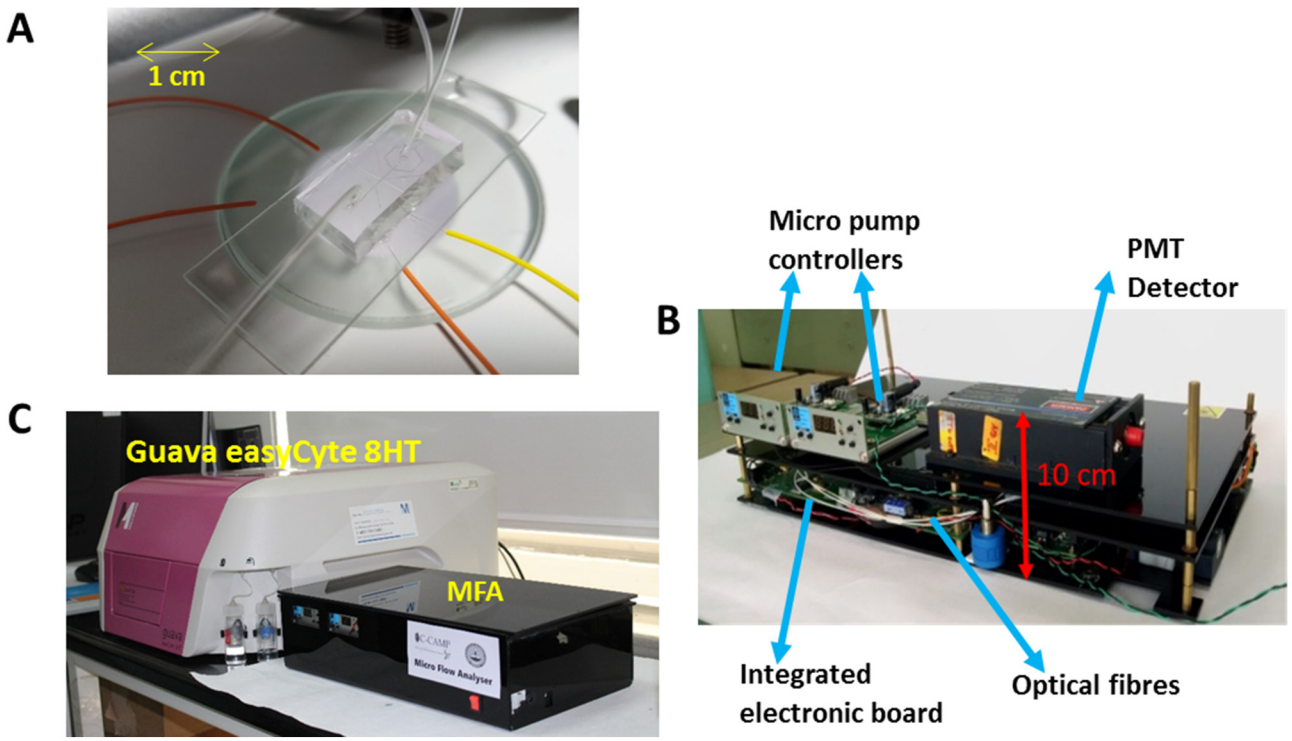

FIG. 3. Typical packaging and assembly of micro-flow analyzer. (a) View of one of the microchips connected to tubing for sample flow and optical fibers. (b) MFA components including laser, detectors, data acquisition board (ZedBoard), optical fibers and micropumps. (c) Size comparison of the MFA with Guava® easyCyte 8HT machine. Dimension of our device is $39 \times 22 \times 10\,\text{cm}^3$.

fluorescence intensities with different lasers and with different dye concentrations. To further demonstrate the use of the MFA for diagnostic purposes, we used human blood samples and enumerated CD4 T lymphocyte levels. Since the MFA can count and detect fluorescence from immunostained cells, it can effectively be used for various cell based diagnostic applications including Human Immunodeficiency Virus (HIV) monitoring. Our results on CD4 counting in immunostained blood samples are in good agreement with commercially available bench-top flow cytometers. Thus, we present a consolidated platform for cytometric analysis in a microfluidic chip.

II. OPTOFLUIDIC DESIGN AND OPTIMIZATION

A. The microfluidic flow analyzer (MFA) design

The MFA device fabricated using polydimethylsiloxane (*PDMS*) design uses 2D hydrodynamic focusing of a cell sample into a central fluid flow channel (Fig. 1). The fluid channel is flanked by side grooves for the insertion of optical fibers for light illumination and detection [Figs. 1(a) and 1(b)]. In this PDMS device design, the central fluid channel has a depth of $130\,\mu$m. Fiber grooves on the sides also have the same depth as the fluid channel. Complete insertion of optical fiber ($125\,\mu$m diameter) into the groove ensures that the core of the fiber is aligned with the center of the fluid channel [Figs. 1(c) and 1(d)]. It, thus, removes the need of any further optical alignment.

The design also brings the optical fiber tip to a distance of $150\,\mu$m from the sample stream, matching the working distance of the lens end, and allows controlled illumination of cells in a small cross section of the channel. The light scattered off the cells is then collected at desired angles for simultaneous measurement of different optical parameters of interest. One can also multiplex lasers and detectors without the need of any precision alignment. Scattered light, and fluorescence, from cells are collected into optical fibers coupled to detectors (photo-multiplier tube—PMT), and further processed by a data acquisition board (Fig. 2).

Syringe pumps were used for experiments in lab. Micropumps[29,30] with proper flow optimizations can be used for miniaturized prototype setup. The final dimensions of such a bench-top instrument is expected to be $40 \times 22 \times 10\,\text{cm}^3$, as shown in Fig. 3.

B. Optimization of fiber optics

Standard single-mode optical fibers have $250\,\mu$m buffer diameter and $125\,\mu$m cladding diameter. The buffer coating of the fiber was removed from the tip for easy insertion of the fiber into the grooves of $130\,\mu$m depth. The single mode lensed fiber with $9\,\mu$m core diameter

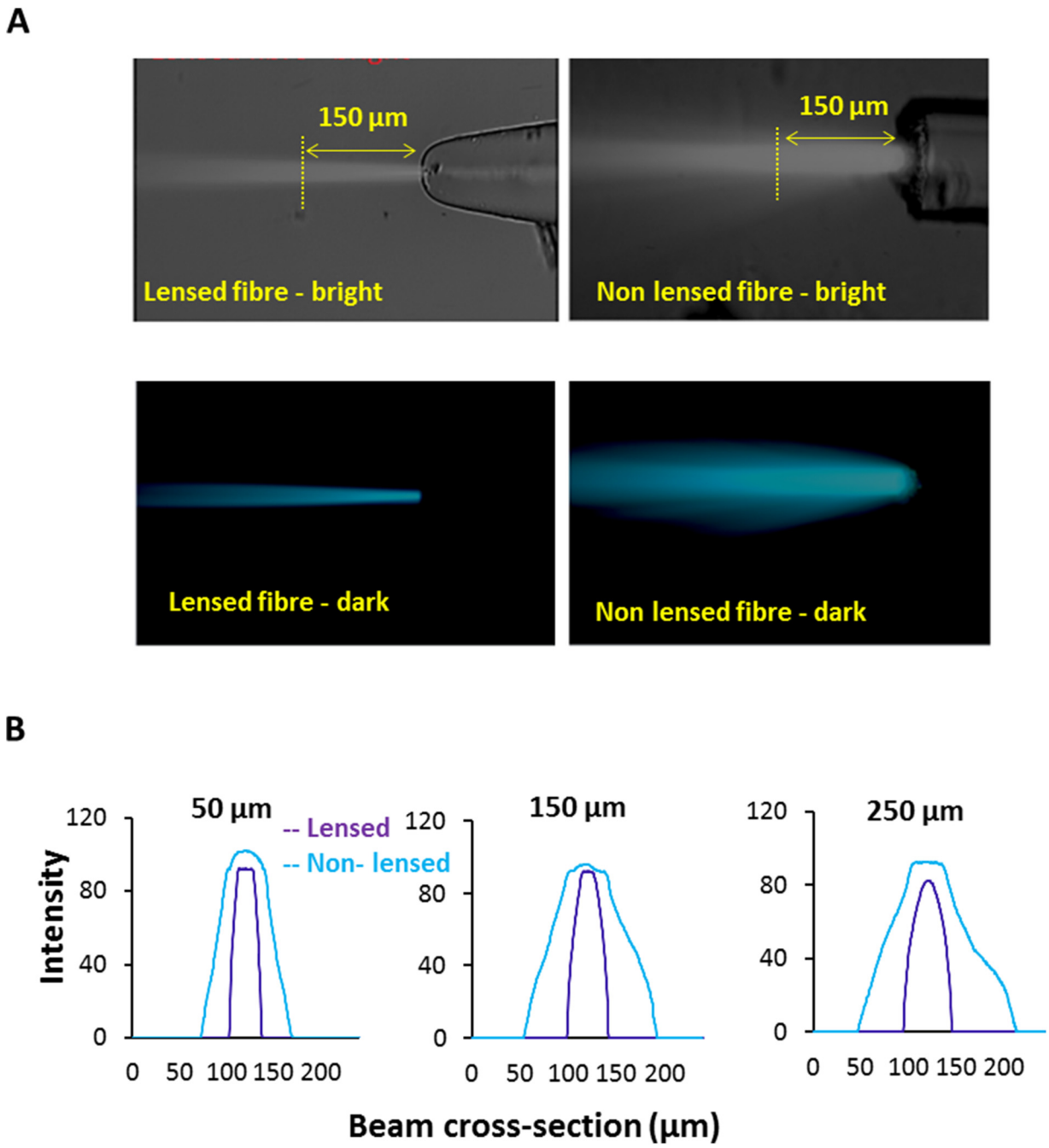

FIG. 4. Beam profile from lensed and non-lensed fibers. (a) Laser beam profile of lensed vs non-lensed optical fibers (microscopic image at 20× magnification). (b) Intensity of light across a laser beam cross-sectional area at different distances from the source fiber tip.

has a tapered tip with a hemispherical curvature. It is designed for focusing the light with 0.47 numerical aperture (NA) at a working distance of 150 μm. Multimode fibers with NA = 0.275, having a higher core diameter (62.5 μm), were used as non-lensed fibers.

The beam profiles of both lensed and non-lensed fiber outputs were compared using microscopic imaging [Fig. 4(a)]. A 488 nm laser output of 500 μW was coupled into both the fibers with their tips immersed in a fluorescent dye drop kept on a glass plate. The

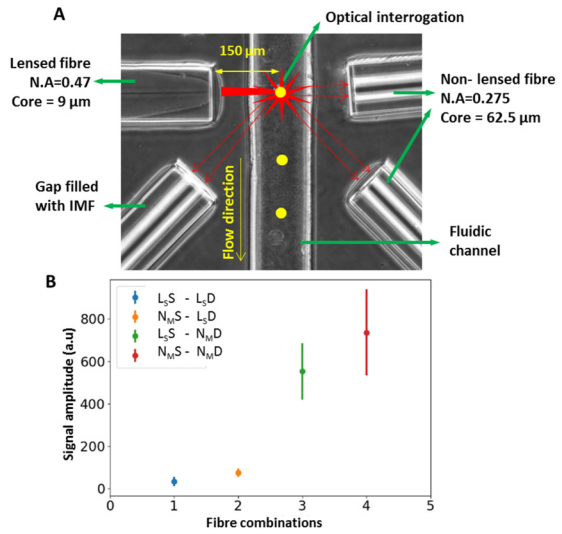

FIG. 5. Optical fiber setup. (a) Microscope image of the fiber setup for optical interrogation. Fiber channels are filled with index matching fluid (IMF) before inserting the fibers to minimize scattering due to air gap. Low core diameter and higher NA (numerical aperture) of the lensed fiber (left) gives tight confinement of the laser light indenting on the cells. Higher core diameter of the detection fiber helps collecting maximum light into the coupled detectors. (b) Scatter signal captured using different combinations of source and detector fibers depicted as median and variance of the scatter amplitude. L_S—single mode lensed fiber, N_M—multimode non-lensed fiber, S—source, and D—detector.

dye fluorescence illuminated the path of light. The intensity profile across the beam was measured using a software tool ImageJ for increasing distances from the tip. Non-lensed fibers show a divergence of light from the tip as measured by an increase in beam width with increasing distances from the fiber tip. However, lensed fibers do not show a significant divergence and provide a narrower beam width [Fig. 4(b)].

We tested different combinations of single mode lensed (L_S) and multimode non-lensed fibers (N_M) as source (S) and detector (D). Index matching fluid (IMF) was used to fill the air gaps around the fiber tip within the groove to minimize scattering losses and hence reduce the optical loss. The required combination of optical fibers were then inserted in the side grooves [Fig. 5(a)]. Scatter data from beads were collected at 45° with all four combinations of fiber as follows: $L_SS - L_SD$ denotes single mode lensed fiber used as both source and detector fibers. $L_SS - N_MD$ denotes single mode lensed fiber used as the source fiber and multimode non-lensed fiber used as the detector fiber. $N_MS - L_SD$ denotes multimode non-lensed fiber used as source fiber and single mode lensed fiber used as detector fiber. $N_MS - N_MD$ denotes multimode non-lensed fiber used as both source and detector fiber. The median and variance of the scatter amplitudes are plotted in Fig. 5(b). From the data, we find that the lensed fiber, when used for detection, cannot collect sufficient amount of light even though it gives less variance in the collected signals, whereas a multimode fiber when used for detection provides higher light collection capacity due to its larger core diameter. On comparing the variance among $N_MS - N_MD$ and $L_SS - N_MD$, the later becomes an

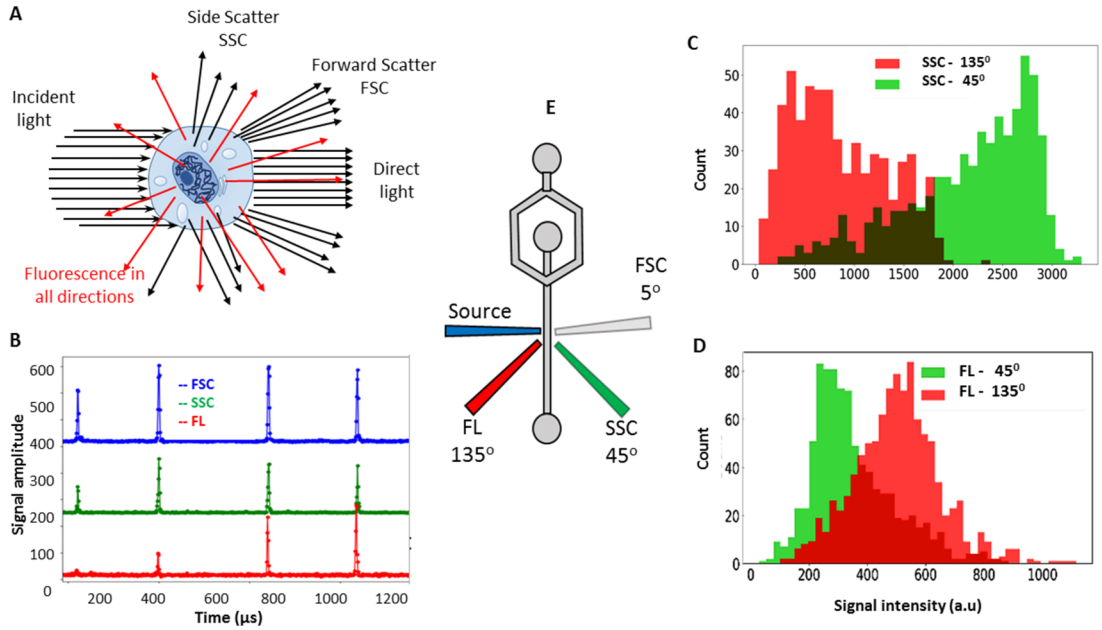

FIG. 6. Understanding scatter and fluorescence signals. (a) Light scatter and fluorescence emission from a cell due to incident light. (b) Representative FSC, SSC, and FL data collected from fluorescent labeled polystyrene beads. (c) Evaluation of SSC acquisition at 45° and 135° detection angles. (d) Evaluation of FL acquisition at 45° and 135° detection angles. Red and green colors correspond to 135° and 45° detection angles to incident light as shown in (e).

appropriate choice. Thus, a single mode lensed fiber L_S serves better for illuminating the cells, and the multimode non-lensed fiber N_M does better at collecting light. Hence, we chose the combination of $L_S S - N_M D$ for our experiment.

C. Acquisition of scatter and fluorescence signals

To measure the FSC, SSC, and FL parameters from cells flowing through the central channel of MFA, we included three grooves for the insertion of detector optical fibers at 5°, −45°, and -135° with respect to the axis of incident light [Fig. 6(b)].

When a cell/particle passes through the incident light, FSC and SSC and FL signals are measured as an increase in photon count at the respective PMT detectors [Fig. 6(b)]. SSC signal intensities for 10 μm nonfluorescent beads were compared at 45° and 135° detection angles. Similarly, the FL signal intensities were also measured at the two angles using fluorescent-tagged beads. A comparison of the median signal intensity at the two detection angles showed that 45° is better for SSC signal while 135° works better for a FL measurement [Figs. 6(c) and 6(d)]. This to the Mie scatter theory[31] confirms where the scatter at a forward angle of 45° has a higher magnitude than the backward angle of 135°.

The following analysis of light scattered by a particle in the microfluidic device supports our experimental findings. The angular dependence of scattered intensity was plotted using a Mie scatter[31] algorithm for a Gaussian beam.[32] We assume a Gaussian beam of waist 6.54 μm (Appendix A) to be incident on a 10 μm polystyrene bead of refractive index 1.4, surrounded by water. Figure 7 summarizes our analysis of the normalized Mie scattered intensity for all angles, $0 < \theta < 180°$. The drawing illustrates the shift in the cone of light, as seen by the multimode fiber (MMF), due to refraction at the flow channel interface. The light cone received into the MMF is limited by the acceptance angle of the fiber, even as the optical intensity is inversely proportional to the

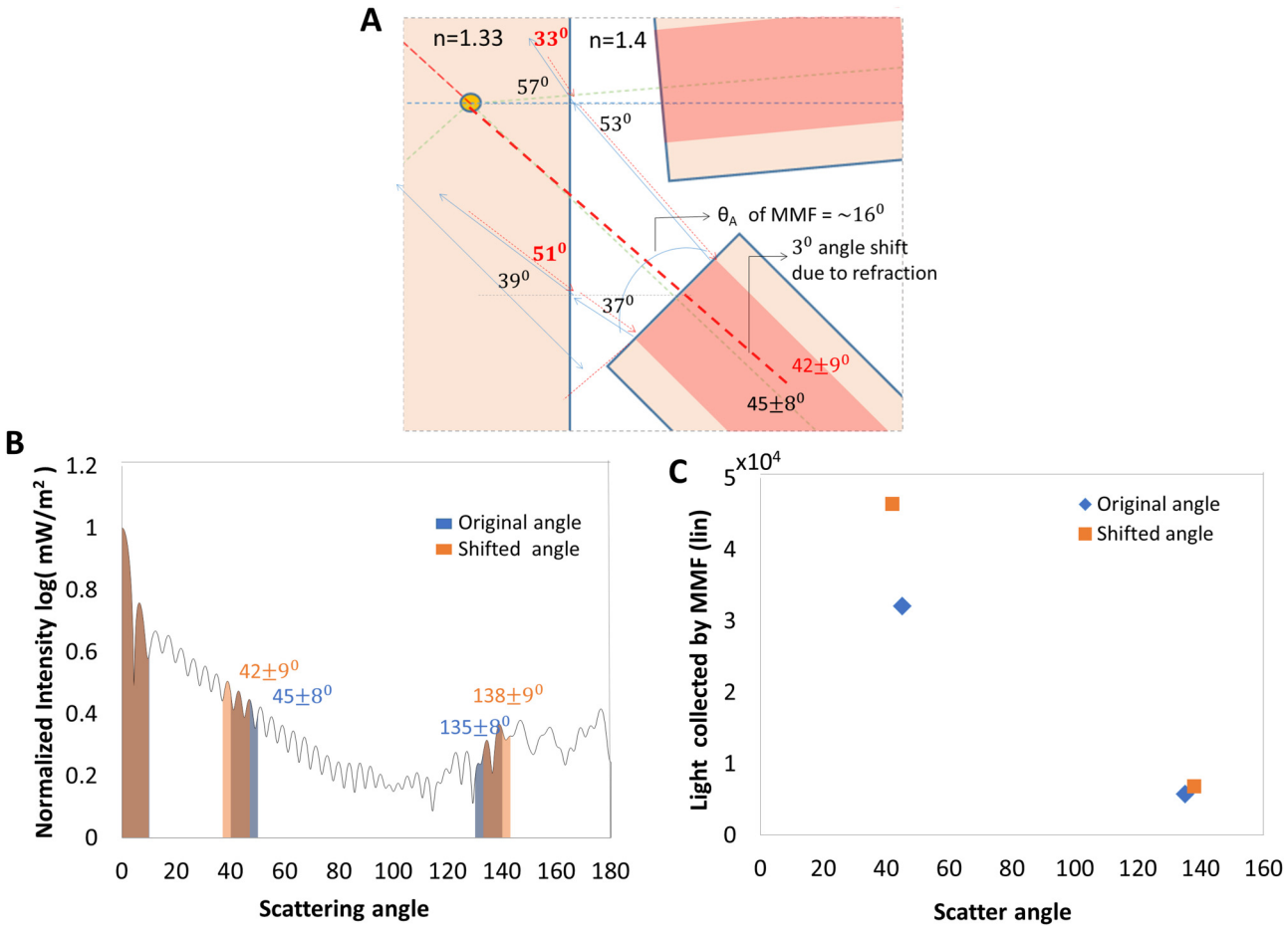

FIG. 7. Light scattering by micro-particle into large detection angles. (a) Drawing illustrating the shift in scatter detection angle due to refraction at PDMS–water interface of microfluidic device. (b) Mie scatter simulation of micro-particle with a Gaussian beam. (c) Effect of optical refraction on the light collected by MMF at large angle detection channels. Angle shift due to refraction is calculated and the resultant difference in collected light is estimated from the area under the shaded region of (b).

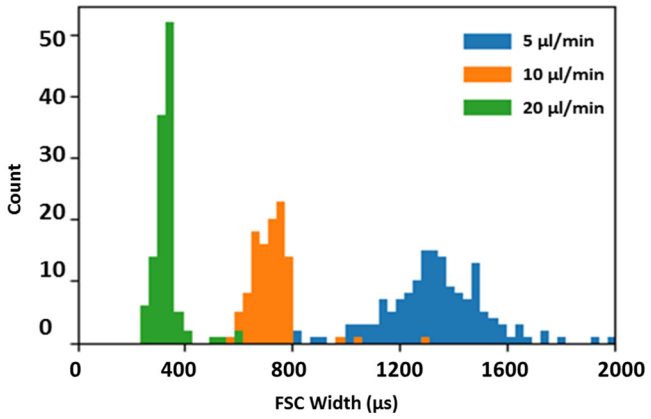

FIG. 8. FSC-width signal reduces proportionally with increasing flow rate corresponding to a reduction in time traversed across the laser beam.

square of distance between the scatterer and fiber. For a fiber kept in the 5° detection channel, the distance from the scatterer is 150 μm. Intensity of incident light getting coupled into this angle is reduced by increasing the distance of the fiber from the fluid channel as demonstrated in Appendix B. However, for the 45° channel, the distance is 230 μm, constrained by the planar geometry of the microfluidic device. This extra distance causes a reduction of intensity by a factor of 2.3 in the 45° channel compared to the 5° channel. But, this drop in intensity is mitigated by the refraction of light at the fluid–PDMS interface, which results in the MMF collecting more light in the 45° channel.

The MMF has an acceptance angle of $\pm 8°$, corresponding to a numerical aperture of 0.275. In Fig. 7(a), we traced the cone of rays centered at 45°, going backward from the MMF into the flow channel with an angular spread of $45 \pm 8°$. Refraction at the PDMS–fluid interface alters the central angle and angular spread to $45 \pm 9°$. Similarly, light collected at $135 \pm 8°$ is shifted due to refraction into a collection angle of $138 \pm 9°$. Figure 7(c) is a plot of the total light collected, estimated as the area under the shaded portion of the Mie scatter intensity in Fig. 7(b). We find that the light collected into the MMF increases due to refraction at 45°, thus making it the preferred angle for detection of SSC.

III. RESULTS AND DISCUSSION

A. Size resolution of beads based on scatter signal

The width of the FSC signal peak is proportional to the time duration for which a flowing particle scatters the incident light. An incremental increase in the sample flow rate resulted in a corresponding reduction in the traverse time that was measured as a decrease in the full width half maximum of the FSC signals (Fig. 8).

Larger particles scatter more light resulting in bigger peaks in the detector output, measured as the FSC-height (FSC-H) signal. Similarly, larger particles also give slightly higher side scatter at large angles measured as SSC-height (SSC-H). Polystyrene micro-beads show increasing FSC-H and SSC-H signals corresponding to increase in bead size are shown in Fig. 9.

We observe a close correlation of the results with same samples run on a capillary based, bench-top commercial cytometer Guava® easyCyte 8HT flow cytometer (Merck Millipore Inc.). The table in Fig. 9(c) quantifies what we see within the boxes in Fig. 9(a). The diagonal values in the table represent the percentages of correctly identified bead sizes, while the off diagonal elements represent the percentage of false classifications, e.g., neither instrument falsely classifies a 3 μm bead (actual size) as a 10 μm bead (identified size). The MFA has about 2% more false classifications than the Guava® easyCyte. This is expected as the MFA works only with a 2D hydro-dynamically focused sample, where beads could have some variation in the vertical plane.

B. Fluorescence measurement from cells

Fluorescence intensity associated with specific fluorophores/fluorescent tags present in a cell are often used to study and separate different biological populations of interest. To characterize the ability of the MFA to resolve different fluorescent intensity levels, we used monocytic cells stained with different dyes at increasing concentrations. Cells stained with Rhodamine 123 dye (excitation/emission 488/530 nm) at 0, 1, and 5 μg concentrations were well separated by MFA. This fluorescence intensity measurement was comparable to that of Guava®easyCyte 8HT with equal number of events collected [Figs. 10(a) and 10(b)].

To check MFA functionality at another wavelength and the sensitivity of our flourescence photon counter, we stained the cells with UV excitable Hoescht dye at varying concentrations of 0, 1, and 10 μM. The MFA was able to pickup increasing blue fluorescence levels from Hoescht stained cells, as seen in Fig. 11. In the earlier experiment, fluorescent staining was with Rhodamine dye, a cytoplasmic dye excited by a 488 nm blue laser and emitting light in green. On the other hand, Hoechst is a nuclear staining dye excited in the UV range and emitting blue fluorescence upon incorporation in the DNA. Thus, Figs. 10 and 11 demonstrate the functionality of MFA across a wide range of optical spectra. The two experiments also demonstrate that the MFA can be easily customized for use with different lasers, detectors based on experimental requirements.

C. CD4 immunostaining in blood samples

From the onset, the MFA was developed keeping in mind the requirements for diagnostic testing of biological samples. One such application is monitoring of CD4+ T lymphocyte count in HIV patients. Regular immune health monitoring of patient blood samples for CD4 T lymphocytes is critical for effective anti-retro viral therapy (ART)24. However, in many places in underdeveloped and developing countries, regular immune health monitoring is a challenge due to nonavailability of flow analyzers. Many patients remain undiagnosed and several others do not get timely ART doses. To overcome this challenge, we tested the functionality of the MFA for CD4 immunostaining of human T lymphocytes.

SupT cells (ATCC human T lymphocyte cell line) were incubated with primary antibody against human CD4 molecules followed by Alexa-48 labeled secondary antibody. The MFA was successfully able to estimate the fluorescence signal of stained cells

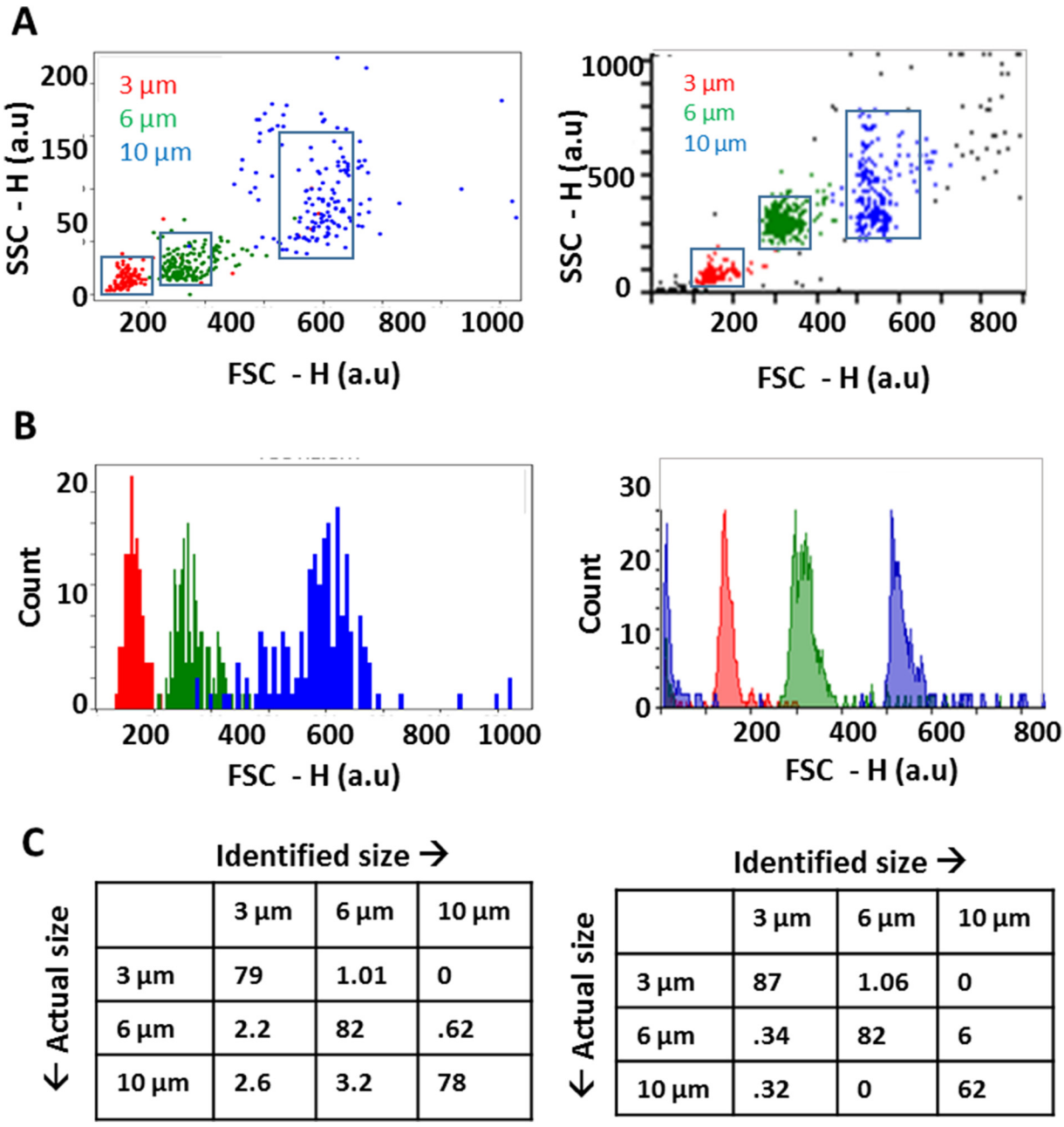

	3 µm	6 µm	10 µm
3 µm	79	1.01	0
6 µm	2.2	82	.62
10 µm	2.6	3.2	78

	3 µm	6 µm	10 µm
3 µm	87	1.06	0
6 µm	.34	82	6
10 µm	.32	0	62

FIG. 9. Particle size discrimination based on FSC and SSC signals. (a) FSC-height vs SSC-height data for beads of 3 μm, 6 μm, and 10 μm comparison of data obtained in MFA (left panel) with the data from Guava® easyCyte machine (right panel). (b) Histogram of FSC-height signal for 3 μm, 6 μm, and 10 μm polystyrene beads. (c) Percentage of beads identified within the clusters of different sizes associated with.

above the background signals obtained from unstained cells [Fig. 12(a)]. We further tested the capability of the MFA in counting CD4 cells in blood samples. Healthy patient blood samples were collected from a blood bank, red blood cells (RBCs) were lysed and the remaining white blood cells (WBCs) were immunostained with CD4 antibodies and analyzed on the MFA. The results were compared against those obtained from the Guava®easyCyte flow cytometer, the latter being a WHO certified bench-top

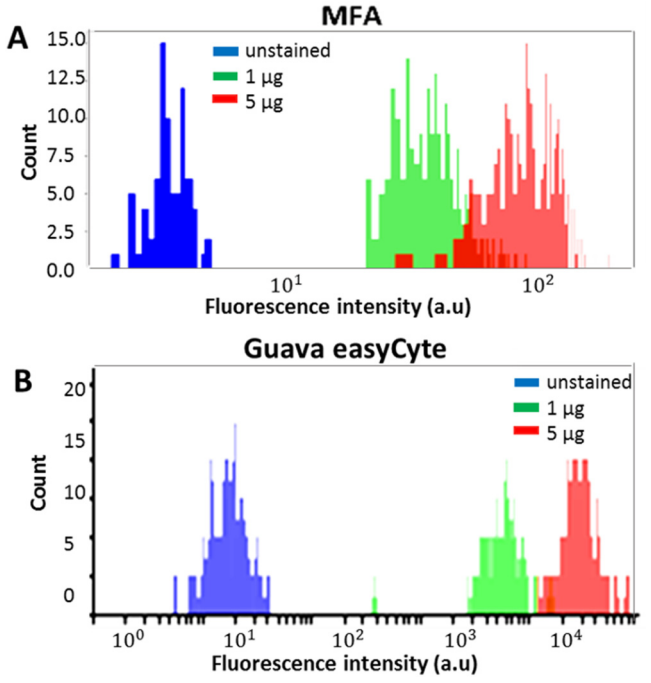

FIG. 10. Fluorescence intensity profiles of cells stained with different concentrations of Rhodamine 123 dye in (a) MFA and the (b) Guava®easyCyte flow cytometer.

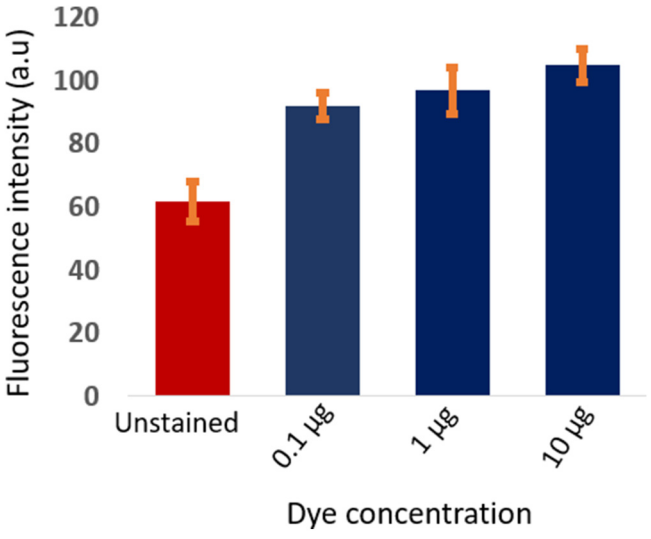

FIG. 11. Sensitivity of the blue fluorescence measured for increasing concentrations of the Hoescht dye, after staining of cells. The error bars mark the standard deviation in the fluorescence signals measured over the stained and unstained cell population.

analyzer for HIV (Human Immunodeficiency Virus) monitoring in resource-limited settings.[33] The number of CD4 stained cells (FL signal) were counted against the total number of cells analyzed in the sample (FSC signal) to obtain the percentage of CD4 cells in the respective blood sample [Figs. 12(b) and 12(c)]. The MFA results show a good agreement with Guava®easyCyte data as seen in the Bland–Altman plot where the data points lie within 95 % limits of agreement [Fig. 12(d)].

D. Characterizing different cell types in a heterogeneous cell population

To show the capability of the MFA to differentiate a heterogeneous population of cells we have run an experiment with samples of human monocytic cells (THP1) and yeast cells. Figure 13 shows the identification of cells into two populations based on the FSC and SSC width signals.

We set SSC − W = 4 (arbitrary units) as a threshold to count human and yeast cells. We observe 11 % of the human cells (blue) below the SSC − W = 4 line, and 15 % of yeast cells (red) above the line. This separation can be further improved upon by advanced clustering methods.[34] We further demonstrate the use of fluorescence (FL) photon counts to analyze the two different cell types. Since the yeast cells were unstained, they are easily identified and separated from the human cells in a simple histogram (Fig. 13).

IV. MATERIALS AND METHODS

A. System setup

The three major disciplines involved in the experimental system are microfluidics, optics, and electronics with associated software. The microfluidic device principally contains a central flow channel for sample which is hydro-dynamically flow focused into a central stream by the sheath fluid coming in through the sides. The sample and sheath inlets are connected to the syringe pumps (NE 300, New era pump systems Inc.) via silicone tubing with an inner diameter of 0.58 mm (BTPE-90, Instech laboratories Inc.) for fluid injection. Below the flow-focusing junction, the microfluidic device has grooves on both sides of the central flow channel for housing optical fibers (Fig. 1). Optical fibers (Lase Optics Corporation) placed in the grooves/fiber channels are used for the illumination of laser light and collection of optical signals from cells passing through the path of light. The collected light signals are coupled to detectors. Detector signals are acquired by the electronic ZedBoard (Xilinx Zynq-7000) and processed to get scatter and fluorescence values corresponding to individual cells. Figure 1(c) illustrates the workflow of the micro-flow analyzer under testing.

B. Device fabrication protocol

The microfluidic device was prepared from PDMS by standard soft-lithography techniques.[35] The design mold was fabricated on a silicon wafer by UV exposure through a photo-lithography mask and subsequent development. A curing agent was added to the PDMS base (Sylgard 184 silicone elastomer kit; Dow Corning Corporation) to a final concentration of 10 % by weight, mixed and poured over the mold to a depth of 5 mm. Following degassing for

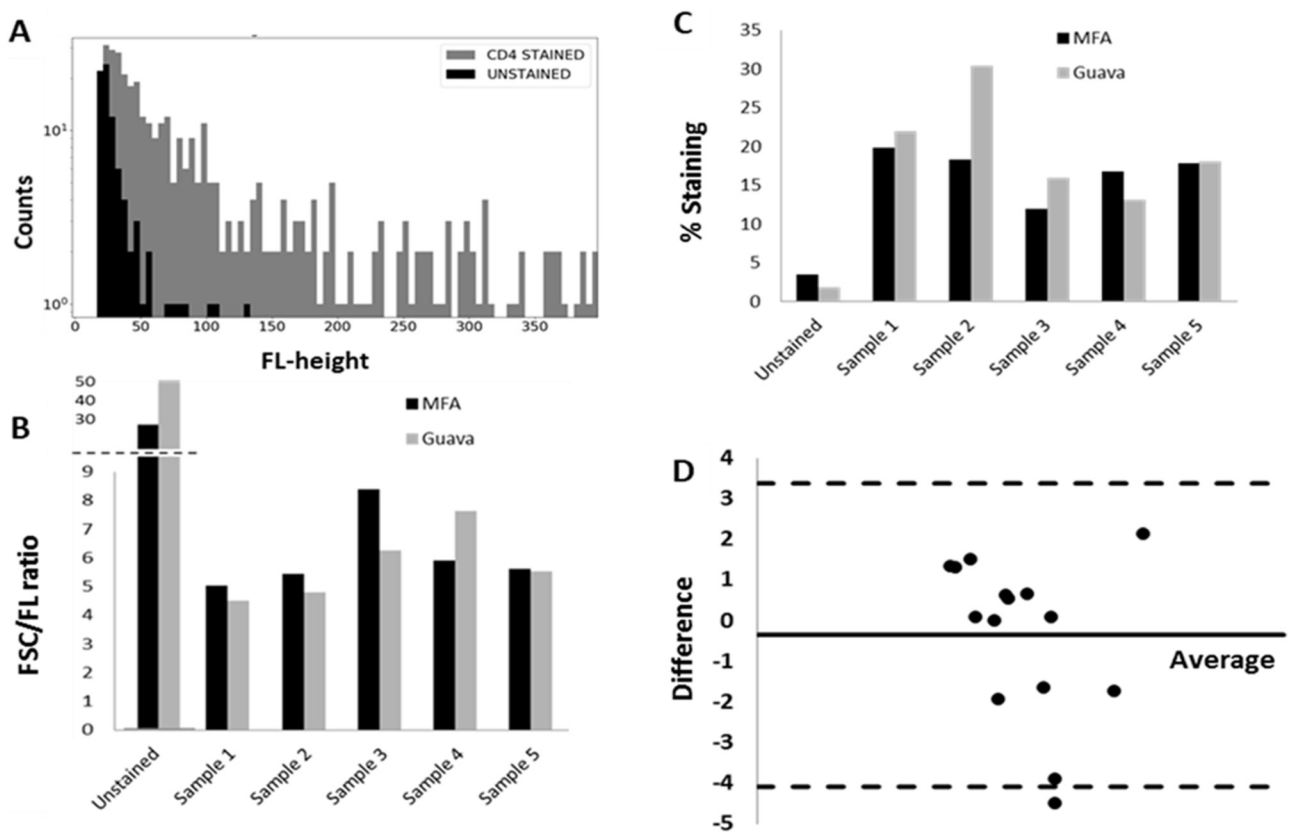

FIG. 12. CD4 analysis of human T cells and blood samples. (a) Fluorescence (FL-height) histogram of CD4 stained and unstained T lymphocytes in MFA. (b) Plot showing the ratio of FSC events to FL events counted for unstained and CD4 stained blood samples in MFA and Guava. (c) Percentage of CD4 stained cells in blood. (d) Bland–Altman plot for differences in FSC/FL events ratio observed between Guava®easyCyte and MFA (n = 15). MFA data lie well within the 95 % limit of agreement.

several minutes and cross-linking at 65°C for 3 h, the PDMS was peeled off the mold and the inlet and outlet ports were punched with a 1 mm diameter biopsy punch. Another flat PDMS layer of around 1.5 mm thickness was also made as a substrate for bonding the patterned layer with 2 h of curing at 60 °C. PDMS mold and the substrate layer were then carefully cut out in the required dimensions and subjected to the oxygen plasma treatment (Harrick plasma cleaner) with patterned side facing up and the substrate layer adjacent to it for 30 s. The cured PDMS samples were then treated with Rain-x and left overnight for reducing the hydrophobicity before testing it with any fluid.

C. Hydrodynamic flow focusing

Syringe pumps control the flow of sample and sheath fluid from their respective inlets to the central microfluidic channel. Sheath fluid flowing along with the sample stream on both the sides develops hydrodynamic flow focusing. The velocity of the sheath fluid can be used to control the width of the sample stream by changing the relative flow rates of the sample and sheath. A sample prepared to a final concentration of 10^6 cells/ml with flow rates in the range of 10– 50 μl/min was used to obtain single cell events at the point of interrogation.

D. Fibre coupled optical detection system

A single mode (SM) optical fiber with 9 μm core diameter, 125 μm cladding diameter (LF-SM-SC-01-SMF-28-FC/APC, Lase optics Corporation) with an engineered lens tip (Lase Optics Inc.) with a numerical aperture (NA) of 0.47 was used for light focusing. Scattered signals and fluorescence were detected using normal multimode (MM) fibers (62.5 μm core diameter, 125 μm cladding diameter) with a higher mode field diameter (100 μm) for higher optical coupling. Any losses due to refractive index mismatch inside the fiber channel were minimized by using index matching fluid (IMF) of $n = 1.4$ which is between that of the fiber and the PDMS. Lasers and detectors were chosen depending on the biomarker being analyzed. The 488 nm laser source (SLOC lasers) was used at 5 mW with a photo-multiplier tube (PMT—Coherent Inc.) for detection of FSC, SSC, and FL. Neutral density filters and band-pass filters were used with the PMTs to obtain light of required power and wavelength.

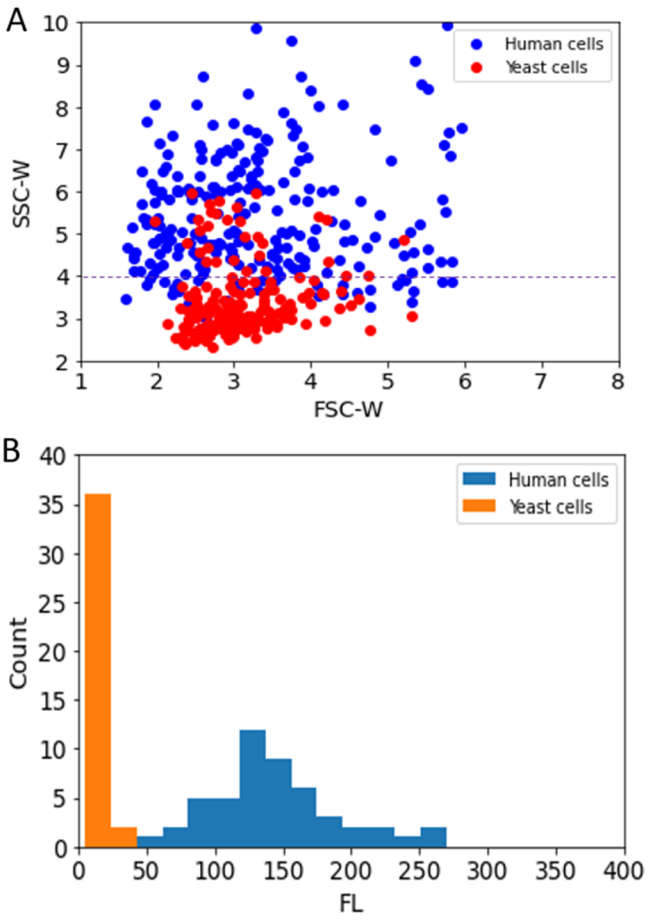

FIG. 13. (a) Identifying different types of cells based on FSC and SSC widths. (b) Observed fluorescence photon counts for stained human and unstained yeast cells.

E. Signal processing

The optical signals being generated at the interrogation point are guided to the detectors by optical fibers. On the detector, the incident photons are converted into digital transistor logic (TTL) pulses of 35 ns pulse width and 60 ns dead time. The rate of these TTL pulses generated by the detector is a measure of photon intensity. The FPGA on the ZedBoard is programed to count these fast pulses coming in three channels (FSC, SSC, and FL) every 100 μs. The counting period was chosen to have enough data points per event for sufficient resolution of fast moving micro-particles. For example, the particles flowing at 10 μl/min flow rate through the flow channel cross section of $130 \times 30\,\mu m^2$ would have a velocity of 25 mm/s. Hence, the particle takes 800 μs to traverse 20 μm laser spot. A signal of with 800 μs time width can easily be resolved with 100 μs sampling time.

The resultant FSC, SSC, and FL raw data values were then processed in real-time using a peak detection algorithm written in Python.

(1) A cut-off is set to remove the noise from the signal and a minimum number of data points per peak are allocated for identification of true events.
(2) Event parameters such as peak width and height were extracted after interpolating the data points on each peak. Integration of the event data gave the area under the peak.
(3) Finally, scatterplots and histograms were generated for visual representation and analysis.

F. Sample preparation

Different sized polystyrene beads for standardization were obtained from Bangs Laboratories. Live THP1 monocytic cells (ATCC) were used for staining with fluorescent dyes. THP1 cells were maintained in RPMI media (Gibco) in suspension culture. The cell suspension was centrifuged at 1200 rpm for 5 min, and the cell pellet was re-suspended at a final concentration of 1×10^6 cells/ml along with the desired quantities of cell-permeable fluorescent dyes—DAPI, Hoescht 33342, and Rhodamine 123 (Thermofisher Scientific). Cells were incubated with the dyes for 15 min at room temperature followed by two PBS (phosphate buffered saline) washes before running on the MFA. For CD4 staining, SupT cells (ATCC cat #100) were cultured in RPMI media supplemented with 10% FBS. 1×10^6 cells were incubated with a 1:100 dilution of antihuman CD4 antibody (Clone OKT4) in ice for 15 min. The cells were then washed twice with PBS and incubated with 3:100 diluted Alexa Fluor 488 labeled secondary antibody at ice for 20 min. The samples were washed twice in PBS and re-suspended in FACS buffer (PBS+2 % FBS) for analysis in MFA.

G. CD4 staining of healthy human blood samples

100 μl of whole blood (healthy human blood samples from TTK blood bank, Karnataka with appropriate approvals from the Institute Ethics committee) was incubated with 5 μl human trustain for 10 min at room temperature prior to staining. 10 μl of CD4 APC-Cy5.5 antibody was added to blood and incubated at 4°C for 60 min (dark). 1 × RBC lysis buffer (Roche) was added to blood and incubated at room temperature for 10 min (dark) with intermittent mixing. Samples were centrifuged at 400 g, 4°C for 5 min. Samples were then washed twice with wash buffer (PBS with 2 % fetal bovine serum) and re-suspended in PBS.

V. CONCLUSIONS

We have developed a microfluidic flow analyzer for the optical interrogation of particle size and associated fluorescence signals. The device has been developed keeping in mind the technical requirements for biological cell/sample testing while also ensuring its usability across a wider base in resource-limited settings. This has been mainly achieved by miniaturizing the system using microfluidics along with the novel use of lensed optical fibers for optical interrogation. The lab level prototype was successfully tested for flow optimization, optics integration, signal detection, and data analysis. Use of integrated fiber optics in a microfluidic chip saves a significant amount of space and reduces the overall system bulkiness and complexity. We have eliminated the need of free space

optical components by using customized lensed optical fibers. The lensed fibers are crafted to focus the laser light to a tight beam spot on the flowing stream of particles at the point of detection. Fiber-based lensing of light improves the precision of optical signal acquisition without much additional cost or complexity. It also simplifies the fabrication of the microfluidic device by eliminating the need for expensive high-speed camera attached microscopes or complicated on chip lens systems and wave guides, etc. Such microfluidic chip production can easily be scaled up at low cost in either glass or plastic based on application requirement. Since simple mechanical components are available to couple laser light into the optical fibers, use of fiber technology also provides flexibility in terms of use of different laser sources based on the diagnostic test. Also, the use of fiber Bragg gratins can be an effective replacement for optical filters in future systems.

We have demonstrated the capability of MFA to effectively distinguish different sizes of polystyrene beads and different fluorescence intensities of dye-stained cells. We have also shown the comparison of MFA with the Guava® easyCyte 8HT (Merck Millipore Inc.), another commercially available bench-top flow cytometer approved by WHO for CD4 count in patient samples, to further establish its competency. Simple re-configurations in the design of microfluidic chip as well as laser wavelengths/optical filters can easily facilitate the analysis of a wide variety of biochemical assays and cell samples. Such a microfluidic device will give tremendous impetus to affordable point-of-care diagnostics in resource-limited settings globally. Additionally, this has the potential to be integrated in developed geographies to reduce the burden of healthcare costs. This design and integration has been patented internationally.[36]

AUTHORS' CONTRIBUTIONS

A.M. performed the experiments on the MFA, analyzed the data, prepared figures, and wrote the manuscript. P.G. performed experiments, conceptualized and supervised the study, analyzed the data, prepared figures, and wrote the manuscript. A.P.N. performed the blood immunostaining experiments. T.S. and A.P. conceived, designed the study, supervised the experiments, and reviewed the manuscript. A.M. and P.G. have contributed equally to the work.

ACKNOWLEDGMENTS

The authors would like to thank H. Krishnamurthy, Sudip Mondal, and Feroz Mustafa for many initial invaluable design discussions and on flow analysis. We would also like to thank the microfluidics fabrication facility, C-CAMP and the Centre for Nano science and Engineering (CENSE), Indian Institute of Science, for their assistance in microfluidic chip fabrication and use of their fabrication facility. We also thank Jessica Brainbridge-Smith and Coyin Oh for their early support on the design of the chip. We acknowledge Nilesh Marshkole and Anish Bharadwaj for early design and experiments and Abinya Paramasivam for the FPGA programing. We would like to acknowledge the support of the Biotechnology Industry Research Assistance Council (BIRAC), India for funding the Project Vide Sanction Order No. BT/BIPP/0537/16/11.

APPENDIX A: ESTIMATION OF GAUSSIAN BEAM PARAMETERS IN THE MICROFLUIDIC DEVICE

The laser beam emerging out though the optical fiber follows a Gaussian intensity profile as shown in Fig. 14. Numerical analysis of the beam parameters can be done as follows. When Gaussian beam propagate in free space along the Z direction, then at $Z = Z_0$ where the spot size of the beam is minimum value along the beam axis, is known as beam waist. The beam width $w(z)$ is expressed as the function of distance Z from the source as [Eq. (A1)] and plotted as Fig. 15(a),

$$w(z) = w_0\sqrt{1 + \frac{Z}{Z_R}}, \tag{A1}$$

where the Rayleigh range, i.e., the distance from beam waist where spot size of the beam become $\sqrt{2w_0}$ is

$$Z_R = \frac{\pi {w_0}^2}{\lambda}. \tag{A2}$$

The radius of curvature $R(z)$ is defined for the wave front of the beam and the value will be negative for the converging beam, positive for diverging beam, and infinity at beam waist [Fig. 15(b)],

$$R(z) = Z\left[1 + \left(\frac{Z_R}{Z}\right)^2\right]. \tag{A3}$$

The laser beam in a microfluidic device passes through materials of different refractive indices and thicknesses. Here, the ray tracing and estimation of final beam parameters are found out by using the ABCD matrix method as explained below.

For a Gaussian beam of wavelength λ and radius of curvature R, beam spot size w_0 and in a medium of refractive index n, the complex parameter q is defined as

$$\frac{1}{q} = \frac{1}{R} - i\frac{\lambda}{\pi n w^2}. \tag{A4}$$

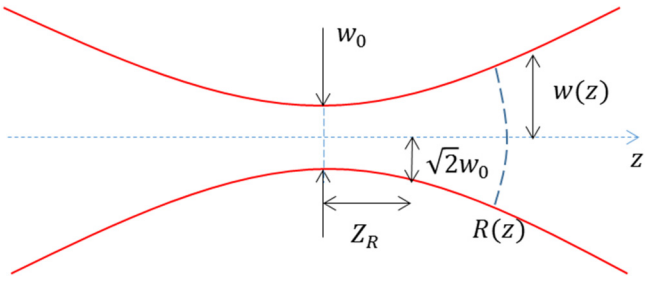

FIG. 14. A schematic showing the parameters of a Gaussian beam.

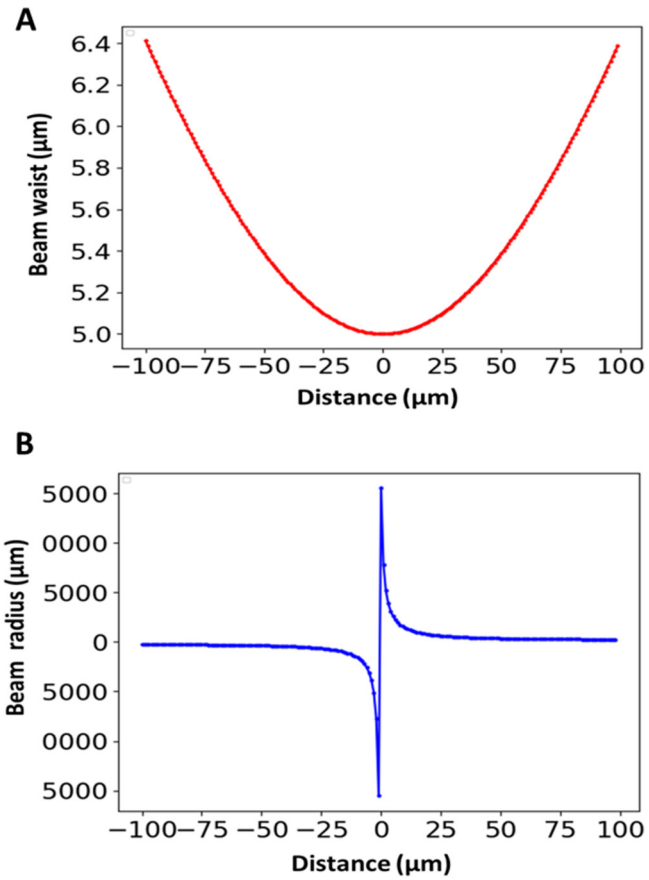

FIG. 15. Beam waist (a) and beam radius (b) of the Gaussian beam plotted as a function of distance Z, from the optical fiber, in free space.

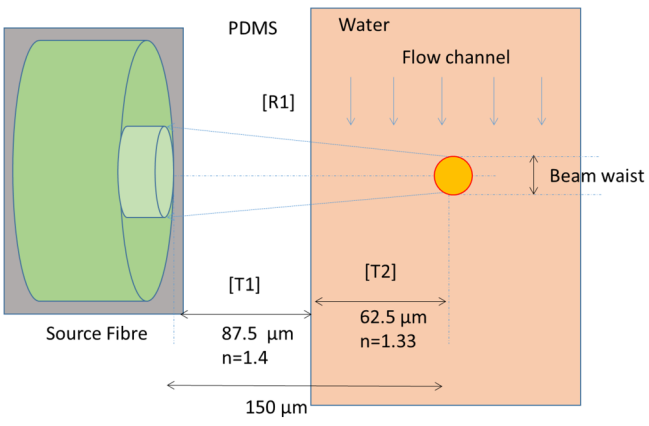

FIG. 16. Schematic showing the material interface though which the optical beam focusing into the microfluidic flow channel.

The entire optical system can be represented as

$$\begin{bmatrix} q_2 \\ 1 \end{bmatrix} = \begin{bmatrix} A & B \\ C & D \end{bmatrix} \begin{bmatrix} q_1 \\ 1 \end{bmatrix}, \tag{A5}$$

where the input and output Gaussian beam parameters q_1 and q_2 are related by the ABCD matrix such that

$$q_2 = \frac{Aq_1 + B}{Cq_1 + D}. \tag{A6}$$

Using the specifications of lensed fiber in free space, we have a spot size of $5\,\mu$m and working distance of $150\,\mu$m (distance from fiber end to beam waist). Thus, q_1 at the waist of the Gaussian beam waist is

$$\frac{1}{q_1} = \frac{1}{0} - i\frac{630\,\text{nm}}{\pi \times 5\,\mu\text{m}^2}. \tag{A7}$$

Now, when this Gaussian beam propagates from optical fiber into the microfluidic flow channel $150\,\mu$m away from the fiber tip, we must also consider the effect of material interfaces on the beam parameters. We formulate an ABCD matrix for this system as shown in Fig. 16.

After the source fiber, propagation of the beam through PDMS material (refractive index $n = 1.4$) of distance $87.5\,\mu$m is represented by the translation matrix [T1] as

$$[T1] = \begin{bmatrix} 0 & \frac{d}{n} \\ 0 & 1 \end{bmatrix} = \begin{bmatrix} 0 & \frac{87.5}{1.4} \\ 0 & 1 \end{bmatrix}. \tag{A8}$$

When the beam enters the microfluidic flow channel filled with water, the refraction at the PDMS–water interface is given by the refraction matrix [R1] as

$$[R1] = \begin{bmatrix} 1 & 0 \\ 0 & \frac{n_1}{n_2} \end{bmatrix} = \begin{bmatrix} 1 & 0 \\ 0 & \frac{1.4}{1.33} \end{bmatrix}. \tag{A9}$$

Refraction at the fluid channel interface is then followed by translation through water to the center of the fluidic channel, $62.5\,\mu$m away. The translation matrix [T2] is

$$[T2] = \begin{bmatrix} 0 & \frac{d}{n} \\ 0 & 1 \end{bmatrix} = \begin{bmatrix} 0 & \frac{62.5}{1.33} \\ 0 & 1 \end{bmatrix}, \tag{A10}$$

and the ABCD matrix for this system becomes

$$\begin{bmatrix} A & B \\ C & D \end{bmatrix} = [T2]^*[R1]^*[T1]. \tag{A11}$$

From the corresponding ABCD values of the system matrix, we arrive at the following expression for q_2:

$$\frac{1}{q_2} = 51.74 + i79.6. \tag{A12}$$

On comparing Eqs. (A4) and (A12), we get the new Gaussian beam parameters in device as

$$R' = 243\,\mu\text{m}, \tag{A13}$$

$$w_0' = 6.54\,\mu\text{m}. \tag{A14}$$

So, due to the transmission through material interface, the beam parameters at the centre of microfluidic channel gets slightly deviated. The spot size of the beam at the cell interrogation point has increased from 10 μm to 13 μm. The radius of curvature of the beam has become smaller but positive number, which indicates a left shift of the beam waist position in the flow channel by 15 μm. Since we have a Rayleigh range of 130 μm [calculated using Eq. (A2)], the above focus shift is not significant to affect the cell interrogation.

APPENDIX B: FIBER POSITIONING FOR REDUCING THE BACKGROUND COUPLING INTO FSC CHANNEL

The fiber at 5° will allow incident light going into the FSC fiber. To reduce, the amount of incident light, we pull out the fiber to a distance where we get rid of the incident light and can collect FSC reliably. As shown schematically in Fig. 17, the direct light being coupled into the fiber is reduced when the distance of the fiber from the fluid channel, along 5°, is more than 500 μm. Since the receiver fiber is multimode, this small adjustment allows us to avoid the directly incident light and still capture the forward scattered light.

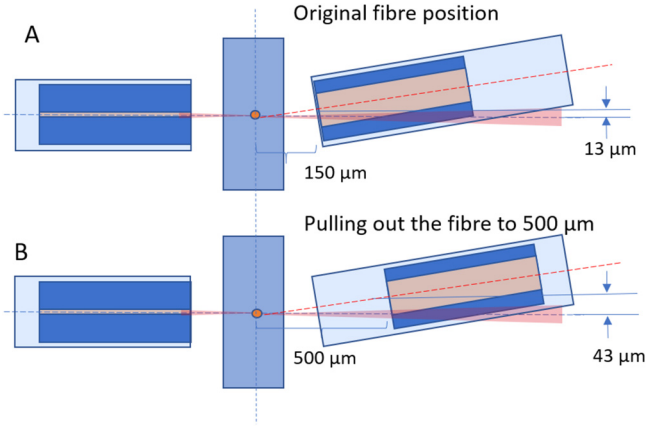

FIG. 17. Optical fiber setup. (a) Original position of fiber where the incident light gets coupled into the fiber. (b) Pulling the fiber away from the tip so that the incident light going into the fiber gets reduced.

DATA AVAILABILITY

The data that support the findings of this study are available from the corresponding author upon reasonable request.

REFERENCES

[1]J. Zhang, X. A. Nou, H. Kim, and G. Scarcelli, "Brillouin flow cytometry for label-free mechanical phenotyping of the nucleus," Lab Chip **17**, 663–670 (2017).
[2]Y. C. Tung, M. Zhang, C. T. Lin, K. Kurabayashi, and S. J. Skerlos, "PDMS-based opto-fluidic micro flow cytometer with two-color, multi-angle fluorescence detection capability using PIN photodiodes," Sens. Actuators B Chem. **98**, 356–367 (2004).
[3]D. Barat, D. Spencer, G. Benazzi, M. C. Mowlem, and H. Morgan, "Simultaneous high speed optical and impedance analysis of single particles with a microfluidic cytometer," Lab Chip **12**, 118–126 (2012).
[4]B. Kim, D. Kang, and S. Choi, "Handheld microflow cytometer based on a motorized smart pipette, a microfluidic cell concentrator, and a miniaturized fluorescence microscope," Sensors **19**, 2761 (2019).
[5]M. Rosenauer, W. Buchegger, I. Finoulst, P. Verhaert, and M. Vellekoop, "Miniaturized flow cytometer with 3D hydrodynamic particle focusing and integrated optical elements applying silicon photodiodes," Microfluid. Nanofluidics **10**, 761–771 (2011).
[6]Z. Wang, J. El-Ali, M. Engelund, T. Gotsaed, I. Perch-Nielsen, K. B. Mogensen, D. Snakenborg, J. P. Kutter, and A. Wolff, "Measurements of scattered light on a microchip flow cytometer with integrated polymer based optical elements," Lab Chip **4**, 372–377 (2004).
[7]R. H. Cole, Z. J. Gartner, and A. R. Abate, "Multicolor fluorescence detection for droplet microfluidics using optical fibers," J. Visual Experiments **111**, e54010 (2016).
[8]X. Mao, A. A. Nawaz, S.-C. S. Lin, M. I. Lapsley, Y. Zhao, J. P. McCoy, W. S. El-Deiry, and T. J. Huang, "An integrated, multiparametric flow cytometry chip using 'microfluidic drifting' based three-dimensional hydrodynamic focusing," Biomicrofluidics **6**, 024113 (2012).
[9]S. Etcheverry, A. Faridi, H. Ramachandraiah, T. Kumar, W. Margulis, F. Laurell, and A. Russom, "High performance micro-flow cytometer based on optical fibres," Sci. Rep. **7**, 5628 (2017).
[10]H. Fallahi, J. Zhang, H.-P. Phan, and N.-T. Nguyen, "Flexible microfluidics: Fundamentals, recent developments, and applications," Micromachines **10**, 830 (2019).
[11]J. Godin, C.-H. Chen, S. H. Cho, W. Qiao, F. Tsai, and Y.-H. Lo, "Microfluidics and photonics for bio-system-on-a-chip: A review of advancements in technology towards a microfluidic flow cytometry chip," J. Biophotonics **1**, 355–376 (2008).
[12]S. Hengoju, S. Wohlfeil, A. Munser, S. Boehme, E. Beckert, O. Shvydkiv, M. Tovar, M. Roth, and M. Rosenbaum, "Optofluidic detection setup for multiparametric analysis of microbiological samples in droplets," Biomicrofluidics **14**, 024109 (2020).
[13]P. Shivhare, A. Prabhakar, and A. Sen, "Optofluidics based lab-on-chip device for in situ measurement of mean droplet size and droplet size distribution of an emulsion," J. Micromech. Microeng. **27**, 035003 (2017).
[14]H. M. Shapiro, *Practical Flow Cytometry*, 4th ed. (John Wiley & Sons, Hoboken, NJ, 1995), Vol. 19.
[15]R. A. Erickson and R. Jimenez, "Microfluidic cytometer for high-throughput measurement of photosynthetic characteristics and lipid accumulation in individual algal cells," Lab Chip **13**, 2893 (2013).
[16]L. Mazutis, J. Gilbert, W. L. Ung, D. A. Weitz, A. D. Griffiths, and J. A. Heyman, "Single-cell analysis and sorting using droplet-based microfluidics," Nat. Protoc. **8**, 870–891 (2013).
[17]A. A. Nawaz, X. Zhang, X. Mao, J. Rufo, S.-C. S. Lin, F. Guo, Y. Zhao, M. Lapsley, P. Li, J. P. McCoy, S. J. Levine, and T. J. Huang, "Sub-micrometer-precision, three-dimensional (3D) hydrodynamic focusing via 'microfluidic drifting'," Lab Chip **14**, 415–423 (2014).

[18]W. Espulgar, Y. Yamaguchi, W. Aoki, D. Mita, M. Saito, J.-K. Lee, and E. Tamiya, "Single cell trapping and cell–cell interaction monitoring of cardiomyocytes in a designed microfluidic chip," Sens. Actuators B Chem. **207**, 43–50 (2015).
[19]D. Jin, R. Connally, and J. Piper, Proc. SPIE **6380**, 140–147 (2006).
[20]Y. Zhao, Q. Li, and X. Hu, "Universally applicable three-dimensional hydrodynamic focusing in a single-layer channel for single cell analysis," Anal. Methods **10**, 3489–3497 (2018).
[21]R. Blue and D. Uttamchandani, "Recent advances in optical fiber devices for microfluidics integration," J. Biophotonics **9**, 13–25 (2016).
[22]M. E. Piyasena and S. W. Graves, "The intersection of flow cytometry with microfluidics and microfabrication," Lab Chip **14**, 1044–1059 (2014).
[23]P. K. Chattopadhyay and M. Roederer, "Cytometry: Today's technology and tomorrow's horizons," Methods **57**, 251–258 (2012).
[24]R. Nunez, "Introduction to the field of cytometry and its importance in biomedicine," Curr. Issues Mol. Biol. **3**, 37–38 (2001).
[25]M. Brown and C. Wittwer, "Flow cytometry: Principles and clinical applications in hematology," Clin. Chem. **43**, 1749–1756 (2000).
[26]F. Venet, A. Lepape, and G. Monneret, "Clinical review: Flow cytometry perspectives in the ICU—From diagnosis of infection to monitoring of injury-induced immune dysfunctions," Crit. Care **15**, 231 (2011).
[27]P. Antal-Szalmás, B. Nagy, I. B. Debreceni, J. Kappelmayer, and J. Kappelmayer, "Measurement of soluble biomarkers by flow cytometry," EJIFCC **23**, 135–142 (2013).
[28]R. S. Abraham and G. Aubert, "Flow cytometry, a versatile tool for diagnosis and monitoring of primary immunodeficiencies," Clin. Vaccine Immunol. **23**, 254–271 (2016).
[29]C.-M. Chang, S.-K. Hsiung, and G.-B. Lee, "Micro flow cytometer chip integrated with micro-pumps/micro-valves for multi-wavelength cell counting and sorting," Jpn. J. Appl. Phys. **46**, 3126–3134 (2007).
[30]T. Ma, S. Sun, B. Li, and J. Chu, "Piezoelectric peristaltic micropump integrated on a microfluidic chip," Sens. Actuators A Phys. **292**, 90–96 (2019).
[31]D. Watson, N. Hagen, J. Diver, P. Marchand, and M. Chachisvilis, "Elastic light scattering from single cells: Orientational dynamics in optical trap," Biophys. J. **87**, 1298–1306 (2004).
[32]See http://www.philiplaven.com/mieplot.htm for calculations for scattering of Gaussian beams.
[33]Merck-Millipore, see https://www.luminexcorp.com/guava-easycyte-flow-cytometers/; accessed 27 December 2019 for "Guava® easycyte™ Flow Cytometer" (2019).
[34]L. M. Weber and M. D. Robinson, "Comparison of clustering methods for high-dimensional single-cell flow and mass cytometry data," Cytometry A **89**, 1084–1096 (2016).
[35]Y. Xia and G. M. Whitesides, "Soft lithography," Annu. Rev. Mater. Sci. **28**, 153–184 (1998).
[36]T. Saiyed, S. Mondal, A. Prabhakar, and H. Krishnamurthy, U.S. patent 9,304,122, Japan patent JP20140555375, S. Africa patent 2014/06473, Russia patent 201400870 (2011).